THE ASTROPHYSICAL JOURNAL, 529:1084–1100, 2000 February 1

HOW MUCH DO HELIOSEISMOLOGICAL INFERENCES DEPEND ON THE ASSUMED REFERENCE MODEL?

SARBANI BASU
Institute for Advanced Study, Olden Lane, Princeton, NJ 08540
M. H. PINSONNEAULT
Department of Astronomy, Ohio State University, Columbus, Ohio 43210
AND
JOHN N. BAHCALL
Institute for Advanced Study, Olden Lane, Princeton, NJ 08540
Received 1999 May 11; accepted 1999 September 16

ABSTRACT

We investigate systematic uncertainties in determining the profiles of the solar sound speed, density, and adiabatic index using helioseismological techniques. We find that rms uncertainties (averaged over the Sun) of $\sim$0.02%–0.04% are contributed to the sound-speed profile by each of three sources: (1) the choice of assumed reference model, (2) the width of the inversion kernel, and (3) the measurement errors. The rms agreement between the standard solar model sound speeds and the best helioseismological determinations is about 0.07%. The profile of the adiabatic index, Γ_1, is determined to an accuracy of about 0.02% with the Michelson Doppler Imager (MDI) data set. The density profile is about an order of magnitude less well determined by the helioseismological measurements. Five state-of-the-art models, each with a significant difference in the input physics or a parameter choice, all give comparably good agreement with global helioseismological measurements. We consider four deficient solar models that are constructed either using old input data, assuming the ^{3}He + ^{4}He fusion reaction does not occur, neglecting element diffusion, or artificially mixing the interior of the Sun. When used as reference models in the inversion process, these deficient models yield sound speeds for the Sun that differ only by 0.1% from the sound speeds obtained using the standard model. We conclude that even relatively crude reference models yield reasonably accurate solar parameters. Although acceptable for most purposes as reference models, nonstandard solar models in which the core is artificially mixed or in which element diffusion is neglected are strongly disfavored by the *p*-mode oscillation data. These nonstandard models produce sound-speed profiles with respect to the Sun that are 4.5 and 18 times worse, respectively, than the agreement obtained with the standard solar model.

Subject headings: Sun: oscillations — Sun: interior

1. INTRODUCTION

Helioseismology has revolutionized our knowledge of the Sun and enriched, stimulated, and largely validated our understanding of the evolution of main-sequence stars with masses comparable to the Sun. The statistical and measurement errors in the best modern samples of helioseismological frequencies have been reduced to tiny fractional values, $\sim$a few $\times 10^{-5}$, which lead to fractional errors in, e.g., the inferred sound velocities that are formally of order 10^{-4} or less.

In this paper we therefore concentrate on systematic uncertainties. The main result of this paper is that the systematic uncertainties in determining the sound speeds are about an order of magnitude larger than the statistical errors.

We need to know quantitatively the accuracy of the solar sound speed and density profiles that are inferred from helioseismology, since these characteristics are often used, e.g., to test opacity calculations (Korzennik & Ulrich 1989; Tripathy, Basu, & Christensen-Dalsgaard 1997), to investigate equations of state (Ulrich 1982; Elliott & Kosovichev 1998; Basu, Däppen, & Nayfonov 1999), and to derive abundance profiles in the Sun (Antia & Chitre 1998; Takata & Shibahashi 1998). Moreover, the precise agreement between the inferred sound speeds and those calculated with a standard solar model used to predict solar neutrino fluxes is a strong argument that solar neutrino experiments require new physics, not revised astrophysics (Bahcall et al. 1997b; Bahcall, Basu, & Pinsonneault 1998).

Solar oscillation data have been inverted to determine the sound speed and density profiles over nearly the entire Sun (e.g., Dziembowski, Pamyatnykh, & Sienkiewicz 1990; Däppen et al. 1991; Antia & Basu 1994; Kosovichev et al. 1997), as well as the adiabatic index, Γ_1 (e.g., Antia & Basu 1994; Elliott 1996; Elliott & Kosovichev 1998). However, helioseismological determinations of solar parameters generally proceed through a linearization of the equations of stellar oscillations around a theoretical reference model of the Sun. We are therefore naturally led to ask the question reflected in the title of this paper: How dependent are the inferred solar characteristics on the assumed reference model?

We have answered this question by constructing a broad range of conceivable modern solar models, each with different input physics or assumptions; we have then used these as reference models to calculate solar sound speeds and densities with different data sets. The range of inferred sound speeds and densities empirically define the systematic uncertainties that are inherent in using reference models to invert helioseismological data.

Five of the solar models are roughly comparable to each other and use physics within the currently acceptable range;

these models are defined in § 3, where they are given the names STD, PMS, ROT, R78, and R508. We also use four different models, each of which is deficient in one or more major aspects of the input physics. The deficient models are also defined in § 3, where they are named OLD, $S_{34} = 0$, NODIF, and MIX.

To explore the systematic uncertainties associated with using a particular data set, we have chosen three different sources of observational data: (1) solar frequencies obtained by the Michelson Doppler Imager (MDI) instrument on board the *Solar and Heliospheric Observatory* (*SOHO*) during the first 144 days of its operation (Rhodes et al. 1997); (2) the set of frequencies obtained by observations of the Global Oscillation Network Group (GONG) during months 4–14 of its observations; and (3) a combination of data from the Birmingham Solar Oscillation Network (BiSON; Chaplin et al. 1996) and the Low-l instrument (LOWL; Tomczyk et al. 1995b). The third set is the same as used by Basu et al. (1997), and it is described in detail there. The MDI and GONG sets have good coverage of intermediate-degree modes. The MDI set has p-modes from $l = 0$ up to a degree of $l = 194$, while the GONG set has modes from $l = 0$ up to $l = 150$. However, both these sets are somewhat deficient in low-degree modes. The BiSON + LOWL combination, on the other hand, has a better coverage of low-degree modes, but has modes from $l = 0$ only up to $l = 99$.

In this paper we concentrate on the properties of helioseismological inversions. We will discuss the implications for neutrino physics in J. N. Bahcall, M. P. Pinsonneault, & S. Basu (1999, in preparation) and explore the results of mixing and rotation on element abundances and helioseismology in M. P. Pinsonneault, S. Basu, & J. N. Bahcall (2000, in preparation).

The present paper is organized as follows. We briefly summarize the inversion technique in § 2, and then describe the solar models used in § 3. Before investigating the systematic uncertainties due to the choice of reference model, we first investigate in § 4 the uncertainties due to the choice of data set, and in § 5 the uncertainties due to the finite resolution of the inversion kernel. We present the inferred solar profiles of sound speed and density in § 6 and Table 2. In § 7 we compare the standard solar model with the helioseismological measurements, and in § 8 we compare the eight variant models with the observations. The dependence of the profiles of the sound speed, the density, and the adiabatic index on the assumed reference model is determined in § 9. We summarize and discuss our principal results in § 10.

2. INVERSION TECHNIQUE

The equations describing linear and adiabatic stellar oscillations are known to be Hermitian (see Chandrasekhar 1964). This property of the equations can be used to relate the differences between the structure of the Sun and the reference model to the differences in the frequencies of the Sun and the model by known kernels. Nonadiabatic effects and other errors in modeling the surface layers give rise to frequency shifts (Cox & Kidman 1984; Balmforth 1992) that are not accounted for by the variational principle. In the absence of a more fundamental method, these surface effects have been treated by the ad hoc procedure of including an arbitrary function of frequency in the variational formulation.

When the oscillation equation is linearized (under the assumption of hydrostatic equilibrium), the fractional change in the frequency can be related to the fractional changes in the squared sound speed (c^2) and density (ρ).

The sound speed (c) used here is the adiabatic sound speed, which is defined as

$$c^2 = \frac{\Gamma_1 P}{\rho}, \tag{1}$$

where Γ_1, the adiabatic index, is defined by the thermodynamic relation

$$\Gamma_1 = \left(\frac{\partial \ln P}{\partial \ln \rho}\right)_s, \tag{2}$$

where P is the pressure and s is the entropy.

We can write

$$\frac{\delta\omega_i}{\omega_i} = \int K^i_{c^2,\rho}(r)\frac{\delta c^2}{c^2}(r)dr + \int K^i_{\rho,c^2}(r)\frac{\delta\rho}{\rho}(r)dr + \frac{F_{\rm surf}(\omega_i)}{E_i}, \tag{3}$$

(Dziembowski et al. 1990). Here $\delta\omega_i$ is the difference in the frequency ω_i of the ith mode between the solar data and a reference model. The kernels $K^i_{c^2,\rho}$ and K^i_{ρ,c^2} are known functions of the reference model that relate the changes in frequency to the changes in c^2 and ρ, respectively, and E_i is the inertia of the mode, normalized by the photospheric amplitude of the displacement. The term $F_{\rm surf}$ results from the near-surface errors.

In this work we have used the subtractive optimally localized averages (SOLA) method (see Pijpers & Thompson 1992) to invert equation (3) in order to determine $\delta c^2/c^2$ and $\delta\rho/\rho$ between a reference model and the Sun. The principle of the inversion technique is to form linear combinations of equation (3) with weights $d_i(r_0)$ chosen so as to obtain an average of $\delta c^2/c^2$ (or $\delta\rho/\rho$) localized near $r = r_0$, while suppressing the contributions from $\delta\rho/\rho$ when inverting for $\delta c^2/c^2$ (or $\delta c^2/c^2$ when inverting for $\delta\rho/\rho$) and the near-surface errors. In addition, the statistical errors in the combination must be constrained. We define the *averaging kernel* as

$$\mathcal{K}(r_0, r) = \sum d_i(r_0)K^i_{c^2,\rho}(r), \tag{4}$$

which is normalized so that $\int \mathcal{K}(r_0, r)dr = 1$. The results of the inversion determine, for example, the difference, δc^2, between the square of the model sound speed and the square of the sound speed of the Sun, i.e.,

$$\delta c^2 = c^2_\odot - c^2_{\rm model}. \tag{5}$$

If the inversion is successful, the relative sound-speed difference can be written as

$$\left(\frac{\delta c^2}{c^2}\right)_{\rm inv}(r_0) \equiv \int \mathcal{K}(r_0, r)\frac{\delta c^2}{c^2}dr \simeq \sum d_i(r_0)\frac{\delta\omega_i}{\omega_i}. \tag{6}$$

The second expression is only approximately equal to the third expression in equation (6) because contributions from the second and third terms in equation (3) cannot be eliminated completely. The weights d_i are determined such that these contributions are substantially less than the error in the solution due to measurement errors in the data. An

expression similar to equation (6) can be written for $(\delta\rho/\rho)_{\rm inv}(r_0)$ as well.

The averaging kernels, $\mathscr{K}$, determine the extent to which we obtain a localized average of $\delta c^2/c^2$ or $\delta\rho/\rho$. The width of the averaging kernel, e.g., the distance between the first and third quartile points, provides a measure of the resolution. Ideally, one would like the averaging kernel to be a δ function at $r = r_0$, but since only a finite amount of data is available, that is impossible to achieve. The effect of finite resolution on the inferred values of $\delta c^2/c^2$ was studied by Bahcall, Basu, & Kumar (1997a) and found to be small for contemporary data sets.

The errors in the inversion results are calculated assuming that the errors in the frequencies are uncorrelated. Thus, the error in $(\delta c^2/c^2)_{\rm inv}$ at radius r_0 is given by

$$\sigma^2(r_0) = \sum_i d_i^2(r_0)\,\frac{\epsilon_i^2}{\omega_i}\ , \qquad (7)$$

where ϵ_i is the quoted error of mode i with frequency ω_i.

The adiabatic index, Γ_1, is related to the sound speed and density (see eq. [1]). Hence, the kernels of c^2 and ρ can be easily converted to those of Γ_1 and ρ (and vice versa; see, e.g., Gough 1993).

The details of how the method is implemented can be found in Basu et al. (1996), and the effects of the inversion parameters on the results are discussed in Rabello-Soares, Basu, & Christensen-Dalsgaard (1999).

3. MODELS USED

We have used a set of nine solar models as reference models to invert the three sets of helioseismological data. Figure 1 compares the computed sound speeds and densities of eight variant and deficient solar models discussed in §§ 3.2 and 3.3 with the sound speeds and densities computed for our standard model (STD), which is described in § 3.1.

Table 1 summarizes some of the key properties of the solar models discussed in this section. For most of the models, the convective zone (CZ) is very close to the observed value of 0.713 ± 0.001 (Basu & Antia 1997). The only models for which the depth of the convective zone is clearly wrong are the NODIF and MIX models. The surface helium abundance of most of the models is also consistent with the abundance determined helioseismologically, 0.248 ± 0.003 (Basu 1998). Only the NODIF model has a helium abundance that is obviously inconsistent with the observed helium abundance.

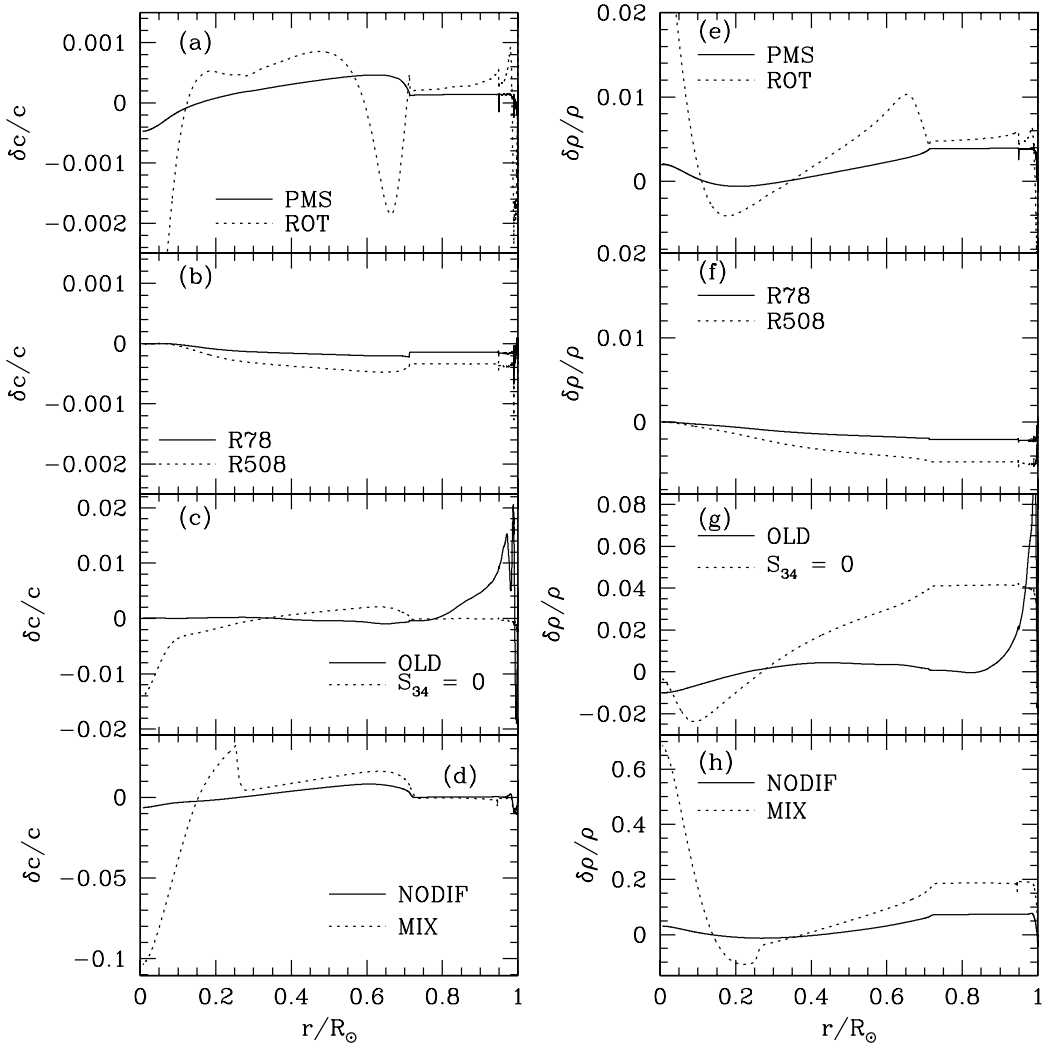

FIG. 1.—Relative sound-speed differences, $\delta c/c$, and relative density differences, $\delta\rho/\rho$, between the standard model (STD) and the other solar models. For each model, $\delta c/c = (c_{\rm STD} - c_{\rm model})/c_{\rm model}$ and $\delta\rho/\rho = (\rho_{\rm STD} - \rho_{\rm model})/\rho_{\rm model}$. The models are described in Table 1. The vertical scales for panels *c*, *d*, *g*, and *h* are larger than for the other panels.

TABLE 1

PROPERTIES OF THE SOLAR MODELS USED

Model	T_c (10^6 K)	ρ_c (g cm^{-3})	Y_s	$r_{cz}/R_\odot$	Comments
STD.....	15.74	152.98	0.2453	0.7123	Standard model; incorporates diffusion; only main-sequence evolution
PMS	15.72	152.73	0.2455	0.7127	Same as STD, but with pre–main-sequence evolution
ROT	15.69	148.30	0.2530	0.7155	Same as STD, but with rotational mixing of elements
R78	15.73	152.97	0.2454	0.7122	Same as STD, but with radius of 695.78 Mm
R508	15.73	152.97	0.2454	0.7121	Same as STD, but with radius of 695.508 Mm
NODIF.....	15.44	148.35	0.2653	0.7261	Same as STD, but with no diffusion
OLD	15.80	154.52	0.2470	0.7111	Old physics (see text)
$S_{34} = 0$	15.62	153.50	0.2422	0.7151	Same as STD, but with reaction constant S_{34} set to 0
MIX	15.19	90.68	0.2535	0.7314	Core mixing (see text)

NOTE.—The first five models listed all use input physics within the currently acceptable range. The last four models are all deficient in one or more aspects of the important input physics.

3.1. *Standard Model: STD*

Our standard model, STD, is constructed with the OPAL equation of state (Rogers, Swenson, & Iglesias 1996) and OPAL opacities (Iglesias & Rogers 1996), which are supplemented by the low-temperature opacities of Alexander & Ferguson (1994). The model was constructed using the usual mixing-length formalism for calculating convective flux. The nuclear reaction rates were calculated with the subroutine *exportenergy.f* (Bahcall & Pinsonneault 1992), using the reaction data from Adelberger et al. (1998) and with electron and ion weak screening as indicated by recent calculations of Gruzinov & Bahcall (1998; see also Salpeter 1954). The model incorporates helium and heavy-element diffusion using the exportable diffusion subroutine of Thoule (Thoule, Bahcall, & Loeb 1994; Bahcall & Pinsonneault 1995).[1]

For the standard model, the evolutionary calculations were begun at the main-sequence stage. The model has a radius of 695.98 Mm. The ratio of heavy elements to hydrogen (Z/X) at the surface of the model is 0.0246, which is consistent with the value observed by Grevesse & Noels (1993). A Krishnaswamy T-τ relationship for the atmosphere was used.

Earlier inversions with similar models have shown that the difference in sound speed between standard solar models and the Sun is small, of the order of 0.1% rms (Bahcall et al. 1997b, 1998; Basu et al. 1997).

3.2. *Variant Models*

In this section, we describe four models that are slight variations on the theme of the standard model.

The PMS model is evolved from the pre–main-sequence stage, but otherwise is the same as STD. The difference in internal structure that results from including the pre–main-sequence evolution is known to be very small (Bahcall & Glasner 1994).

The ROT model incorporates mixing induced by rotation and is a reasonable upper bound to the degree of rotational mixing, which is consistent with the observed depletion of lithium in the Sun (Pinsonneault 1997; Pinsonneault et al. 1999). The initial rotation period for the model is 8 days, which is the median observed value for T Tauri stars (Choi & Herbst 1996). The structural effects of rotation were treated using the method of Kippenhahn & Thomas (1970). Rigid rotation as a function of depth was enforced at all times in convective regions; in radiative regions the transport of angular momentum and the associated mixing were solved with coupled diffusion equations (see § 5 of Pinsonneault 1997). Angular momentum loss from a magnetic wind is included, and then the thermal structure and angular momentum distribution in the interior are used to determine the diffusion coefficients as a function of depth. The angular momentum loss rate and the velocity estimates for the diffusion coefficients are the same as in Krishnamurthi et al. (1997). The parameters of the model, which is started in the pre–main-sequence phase, are fixed by the conditions that (1) the model is required to reproduce the equatorial surface rotational period of 25.4 days; and (2) the model is required to reproduce the observed solar lithium depletion of 2.19 dex (the difference between the meteoritic Li abundance of 3.34 on the logarithmic scale where H = 12, and the photospheric Li abundance of 1.15). The rotational model neglects angular momentum transport by internal magnetic fields and gravity waves; both of these mechanisms can transport angular momentum without mixing and therefore reduce the angular momentum content in the core, decreasing the mixing from meridional circulation and different instabilities. There is evidence from helioseismology that additional angular momentum transport mechanisms, such as gravity waves or magnetic fields, are needed to explain the absence of strong differential rotation with depth in the solar core (see Tomczyk, Schou, & Thompson 1995a).

There has been considerable discussion recently regarding the precise value of the solar radius (see, e.g., Antia 1998; Schou et al. 1997; Brown & Christensen-Dalsgaard 1998) and some discussion of the effects of the uncertainty in radius on the quantities inferred from the helioseismological inversions (see, e.g., Basu 1998). We have therefore considered two models that were constructed with the same input physics as STD, but which have model radii that differ from the radius assumed in constructing STD.

Model R78 has a radius of 695.78 Mm, which is the radius that has been determined from the frequencies of f-modes (Antia 1998). Model R508 has a radius of 695.508 Mm, which is the solar radius as determined by Brown & Christensen-Dalsgaard (1998), who used the measured duration of solar-meridian transits during 1981–1987 and combined these measurements with models of the solar

[1] Both the nuclear energy generation subroutine, *exportenergy.f*, and the diffusion subroutine, *diffusion.f*, are available at: www.sns.ias.edu/~jnb/, under menu item "neutrino software, data."

limb-darkening function to estimate the value of the solar radius. The solar structure is affected only very slightly by the choice of model radii. The fractional differences in the model radii considered in this paper are less than 1 part in 10^3, whereas the radial resolution in the sound speed is at best a few percent (see Fig. 1 of Bahcall et al. 1997a).

The rms sound speed differences between the variant models and the STD model are 0.03% (PMS), 0.08% (ROT), 0.15% (R78), and 0.03% (R508). The average difference (rms) between the four variant models and the STD model is 0.07%.

3.3. *Deficient Models*

In this section, we describe four models that are each deficient in one or more significant aspects of the input physics.

The OLD model is a standard solar model constructed with some relatively old physics: the Yale equation of state (Guenther et al. 1992) with the Debye-Hückel correction (Bahcall, Bahcall, & Shaviv 1968), and old OPAL opacities (Iglesias, Rogers, & Wilson 1992) supplemented with low-temperature opacities from Kurucz (1991). The model does include helium and heavy-element diffusion and uses the nuclear reaction cross section factors (S_0) from Adelberger et al. (1998). In the course of writing this paper, we uncovered a small inconsistency in the code for the Yale equation of state. Fortunately, this inconsistency (which was introduced in recent revisions) does not affect any of our published results, which no longer use the Yale equation of state. For the OLD model, the error in the code causes an increase in the mean molecular weight at a fixed composition of 0.1% relative to the correct value.

The OLD model differs from the STD model in using a cruder equation of state and less precise radiative opacities. Using the old physics rather than the current best input data, as were used in constructing STD, causes significant changes, primarily in the convection zone. This is a typical signature for large differences in the input equation of state, which is the most significant physics deficiency of this model.

For the $S_{34} = 0$ model, the cross section of the nuclear reaction $^3\mathrm{He}(\alpha, \gamma)^7\mathrm{Be}$ was set equal to 0 in order to minimize the calculated neutrino capture rates in the Gallex and SAGE experiments (see Bahcall 1989). This assumption contradicts many laboratory experiments that have measured a cross section for the $^3\mathrm{He}(\alpha, \gamma)^7\mathrm{Be}$ that is competitive with the other way of terminating the *p-p* chain, namely, $^3\mathrm{He}(^3\mathrm{He}, 2p)^4\mathrm{He}$. For the $S_{34} = 0$ model, nuclear fusion energy is achieved in a significantly different way than for the standard solar model, and therefore the calculated solar structure is appreciably different from the standard model (Bahcall & Ulrich 1988). In the standard solar model, about 15% of the terminations of the *p-p* chain involve the $^3\mathrm{He}(\alpha, \gamma)^7\mathrm{Be}$ reaction, whose rate is proportional to S_{34}. If we artificially choose $S_{34} = 0$, then in this model ^{7}Be is not produced, and there are no ^{7}Be or ^{8}B neutrinos.

The NODIF model does not include either helium or heavy-element diffusion. This model therefore represents the state of the art in solar modeling prior to 1992 (see Bahcall & Ulrich 1988; Bahcall & Pinsonneault 1992; Proffitt 1994).

The MIX model has an artificially mixed core. The inner 50% by mass (25% by radius) was required to be chemically homogeneous at all times. All of the other ingredients of the model, including helium and heavy-element diffusion, are the same as in model STD. This model was constructed to be similar to the prescription of Cumming & Haxton (1996), who changed by hand the ^{3}He abundance as a function of radius in the final BP95 (Bahcall & Pinsonneault 1995) solar model in order to minimize the discrepancy between measurements of the total event rates in neutrino experiments and the calculated event rates. Since the Sun evolves over time and Cumming and Haxton only changed the abundances in the final model, we had to adopt some additional prescription regarding how the mixing proceeds as a function of time. We assumed that the mixing was infinitely effective (the core was fully mixed) and constant in time.

The rms sound-speed differences between the deficient models and the STD model are 0.4% (NODIF), 0.2% (OLD), 0.2% ($S_{34} = 0$), and 1.9% (MIX). The average rms difference between the deficient models and the STD model is 0.7%, which is an order of magnitude larger than for the variant models discussed in § 3.2.

4. HOW ACCURATE ARE THE MEASUREMENTS?

How similar are the sound speeds, densities, and values of Γ_1 inferred from different data sets? For sound speeds, this question is answered in Figure 2, which shows the sound-speed difference between the standard model STD and the Sun obtained using the MDI, GONG, and BiSON + LOWL data sets. The results appear relatively similar to the eye, but there are some differences, as large as 0.05%, inside 0.2 $R_\odot$. For densities and Γ_1, the differences between the standard model and the Sun are illustrated in Figure 3.

4.1. *The Sound Speed*

Figures 4*a* and 4*b* reveal even more clearly the differences between the three data sets. In Figure 4 we plot the difference in sound speeds obtained with the GONG and the MDI data and the difference in sound speeds obtained with BiSON + LOWL and MDI. Only one solar model, STD, has been used in all the panels of Figures 2 and 4. The resolution of the inversions obtained with the three data sets is almost the same; hence, the errors due to resolution should be very similar in each set. The only exception occurs near the solar surface, where the fact that the three data sets have different high-degree coverage becomes important. The extent of the high-degree coverage is probably the cause of the systematic differences in the sound speeds that are seen in Figures 2 and 4 near the surface. Elsewhere, differences are caused solely by the measurements.

The errors in the velocity measurements are apparently reasonably well understood; nearly all of the points lie within the 2 σ error bounds delineated in Figure 4. If there were large systematic errors in one of the experiments, then we would expect to see values for $\Delta c/c$ in Figure 4 that fall outside the 2 σ limits. The errors shown in Figure 4 were calculated by combining quadratically at each target radius the errors obtained for inversions of the MDI set and the other sets. The errors at each radius were evaluated as per equation (7).

All data sets yield results for the sound-speed profile that are consistent with each other within the errors of the data sets (cf. Fig. 4). The rms differences are only 0.02% for the sound speeds calculated with the BiSON + LOWL and MDI data sets, and 0.02% for the differences found between

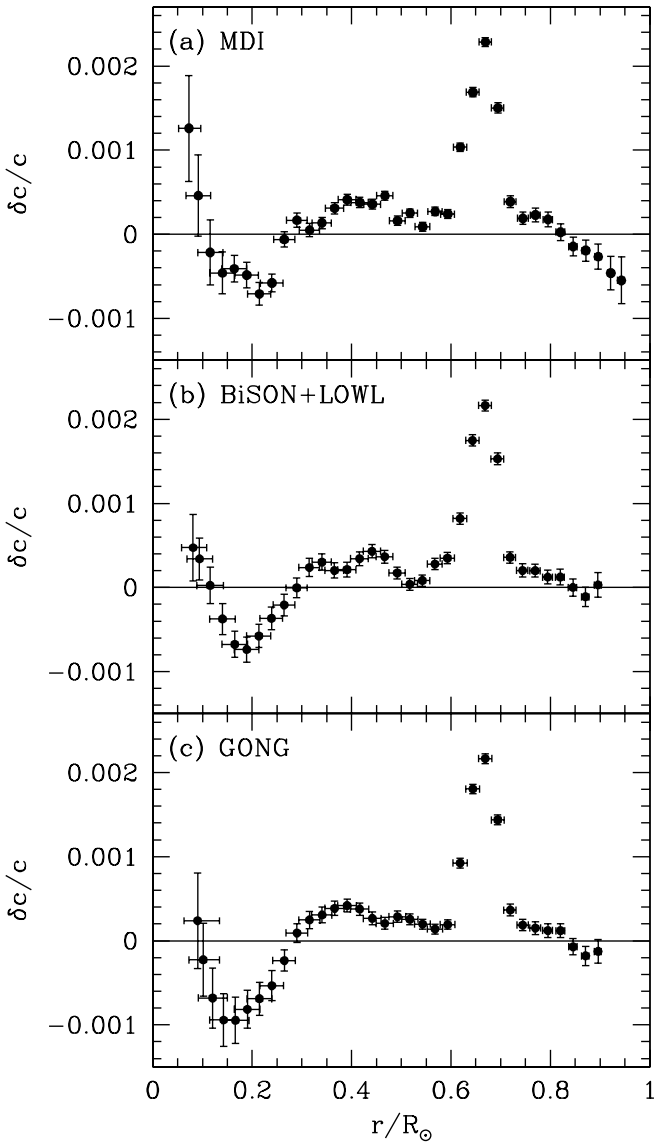

FIG. 2.—Relative sound-speed difference between the Sun and model STD obtained using three different solar oscillation data sets (panels *a*, *b*, and *c*). The differences are in the sense (Sun − model)/model. The vertical error bars indicate 1 σ errors in the inversion results due to errors in the data. The horizontal error bars are a measure of the resolution of the inversion.

the sound speeds calculated with the GONG and the MDI data sets.

4.2. *The Density Profile*

The density profile cannot be determined as precisely as the profile of the sound speed. The primary reason for the reduced precision in inverting for the density profile is that the *p*-mode oscillation frequencies are determined predominantly by the sound speed, with the density contributing only through the perturbation of the gravitational potential. In fact, in the asymptotic limit, the frequencies are determined by sound speed alone. As a result, there is relatively little information about density in the frequencies. A further difficulty that must be overcome in a density inversion is the precise satisfaction of the condition for mass

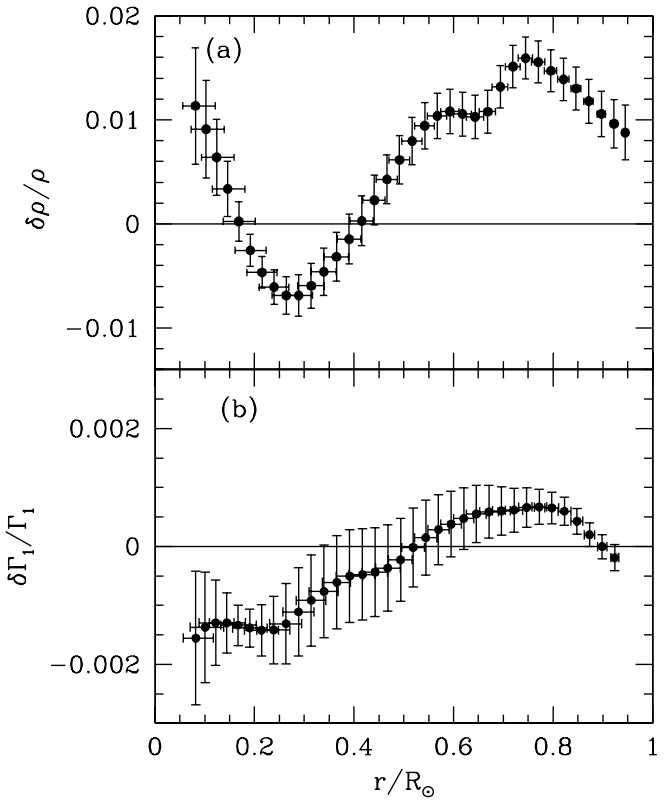

FIG. 3.—(*a*) Relative density differences and (*b*) Γ_1 differences between the Sun and model STD obtained using MDI data. The differences are in the sense (Sun − model)/model.

conservation,

$$\int_0^R 4\pi r^2 \delta\rho = 0 \, . \tag{8}$$

In order to satisfy this condition with high numerical accuracy, the density must be reasonably well determined at all radii. Equation (8) therefore requires a set of oscillation frequencies that includes a large number of low-degree modes (to invert accurately for the core) as well as a large number of high-degree modes (to invert accurately for the surface). If a proper set of either high-degree or low-degree modes is not available, the density inversion becomes very uncertain.

Only for the MDI data were we successful in forming a local averaging kernel that permitted a good inversion for solar density. Figure 3*a* shows that the difference between the density profiles of the solar models and the helioseismologically determined density profile is $\leq 1\%$. However, the accuracy of this measurement is an order of magnitude less precise than for sound speeds.

4.3. *The Adiabatic Index*, Γ_1

The Γ_1 difference obtained between model STD and the Sun is shown in Figure 3*b*. Since most of the Γ_1 difference between the models and the Sun is concentrated at the surface, we use only the MDI data for the Γ_1 inversions. This set has the largest number of high-degree modes.

With the convenient inversion method used here (SOLA), we do not have good spatial resolution close to the surface. There are computationally intensive inversion methods that give superior resolution near the surface; for example, optimally localized averages (see Kosovichev 1995; Elliot &

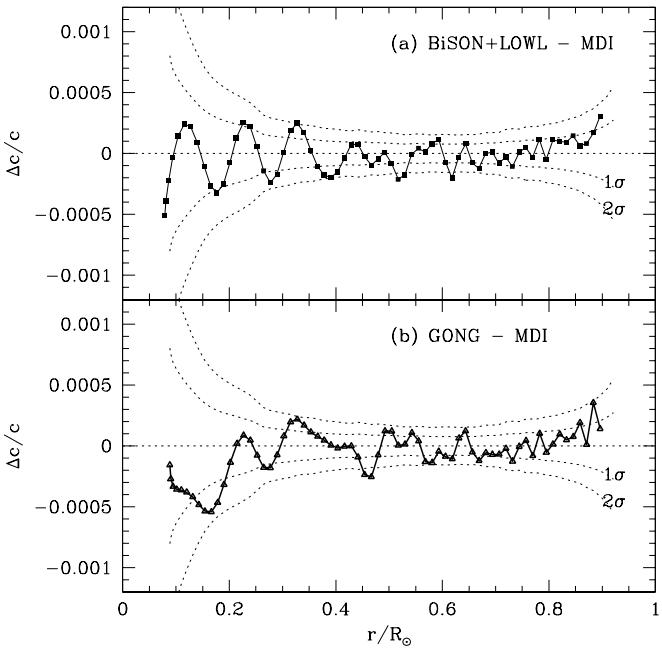

FIG. 4.—Relative errors in the solar sound speed obtained with model STD as the reference model using different data sets. The reference sound speed is taken to be that obtained by inverting the MDI data. The difference between those obtained using BiSON + LOWL and GONG data were calculated. The 1 and 2 σ error envelopes due to errors in the data are shown as dotted lines. Since the reference model was the same for all three inversions, and since the resolutions of the inversions using each of the three data sets are very similar, we do not expect any additional error due to finite resolution or to differences in the reference model. The rms differences are only 0.016% for the sound speeds calculated with the BiSON + LOWL and the MDI data sets, and 0.020% for the differences found between the sound speeds calculated with the GONG and MDI data sets.

Kosovichev 1998; Basu et al. 1999). For the general survey performed in this paper, we did not feel it necessary to invert very close to the solar surface.

The contribution to the solution for Γ_1 from the second function (density, in this case) is more difficult to suppress than for inversions of sound speed or density. Thus, we expect larger errors for reference models with large density differences relative to the Sun.

Given the greater precision of the sound-speed measurements, in the discussion that follows we will emphasize the profile of the sound speed and only refer to the density and Γ_1 profiles for completeness.

5. HOW LARGE ARE THE EFFECTS OF FINITE RADIAL RESOLUTION?

We calculate the solar sound speed using the relative sound-speed difference between the models and the Sun. Thus, if $(\delta c^2/c^2)_{\rm inv}$ is the result of the inversion, then

$$(c^2_\odot)_{\rm inv}(r_0) = \left[\left(\frac{\delta c^2}{c^2}\right)_{\rm inv}(r_0) + 1\right] c^2_{\rm model}(r_0)\ . \qquad (9)$$

However, $(c^2_\odot)_{\rm inv}(r_0)$ is not identically equal to the true solar sound speed, since the inverted speed is an average of the sound-speed difference in the vicinity of r_0. The averaging kernel at r_0, $\mathcal{K}(r_0, r)$, defines the region in r over which the averaging is done. We want to estimate the error introduced into the inferred sound speed by the finite resolution. Since we do not know the true sound speed inside the Sun, we estimate the errors using a solar model as a "proxy Sun." Thus, if $c_{\rm proxy}$ is the sound speed of the proxy Sun, $c_{\rm model}$ is the speed in the reference model, and $\delta c^2/c^2 = (c^2_{\rm proxy} - c^2_{\rm model})/c^2_{\rm proxy}$ is the relative difference between the squares of sound speeds of the two solar models, then the relative error in the inferred sound speed of the proxy Sun due to the finite resolution of the averaging kernel is

$$\left[\frac{\Delta c}{c}(r_0)\right]_{\rm resol} = \frac{1}{2}\left\{\left[\int \mathcal{K}(r_0, r)\,\frac{\delta c^2}{c^2}(r)dr\right] - \frac{\delta c^2}{c^2}(r_0)\right\}. \qquad (10)$$

The factor of $\frac{1}{2}$ in the above expression arises from the conversion of relative errors in c^2 to relative errors in c. Note that $[\Delta c/c(r_0)]_{\rm resol} = 0$ if the averaging kernel $\mathcal{K}(r_0, r)$ is a delta function. The error in density due to the resolution of the density kernel is similarly given by

$$\left[\frac{\Delta\rho}{\rho}(r_0)\right]_{\rm resol} = \left[\int \mathcal{K}_{\rm den}(r_0, r)\,\frac{\delta\rho}{\rho}(r)dr\right] - \frac{\delta\rho}{\rho}(r_0)\ , \qquad (11)$$

where $\mathcal{K}_{\rm den}$ is the averaging kernel obtained for density inversions.

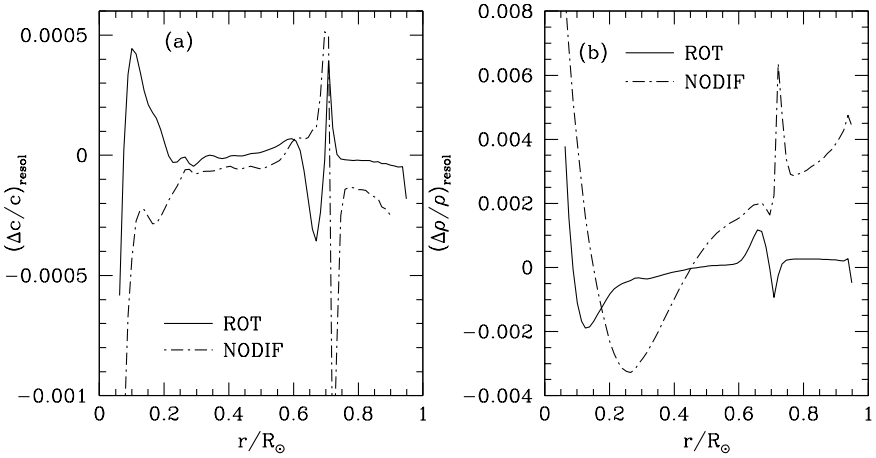

FIG. 5.—Error in the estimated sound speed and density of two models due to the finite resolution of the inversions. In both cases, the reference models used is STD. The quantities $(\Delta c/c)_{\rm resol}$ and $(\Delta\rho/\rho)_{\rm resol}$, defined in eqs. (10) and (11), respectively, are estimates of the errors due to resolution that are expected in the solar sound speeds and density obtained by inversion. The errors are largest where the sound-speed difference between the reference model and the test model shows a sharp gradient, as occurs, for example, at the base of the convection zone.

TABLE 2

SOLAR SOUND SPEED, DENSITY, AND ADIABATIC INDEX (Γ_1), AS DERIVED FROM MDI DATA WITH MODEL STD

$r/R_\odot$	c (cm s^{-1})	σ_c (cm s^{-1})	ρ (g cm^{-3})	σ_ρ (g cm^{-3})	Γ_1	σ_{Γ_1}
6.72421E−02.....	5.11757E+07	3.94099E+04	1.15099E+02	7.07543E−01	1.66474E+00	2.25238E−03
8.09010E−02.....	5.11011E+07	2.73209E+04	1.03410E+02	5.79980E−01	1.66516E+00	1.91496E−03
1.03240E−01.....	5.06842E+07	2.24633E+04	8.56885E+01	3.98898E−01	1.66546E+00	1.52223E−03
1.27841E−01.....	4.97924E+07	1.58364E+04	6.89479E+01	2.37507E−01	1.66557E+00	1.11374E−03
1.52136E−01.....	4.85481E+07	9.44176E+03	5.52090E+01	1.32744E−01	1.66559E+00	7.36144E−04
1.76272E−01.....	4.70638E+07	6.85910E+03	4.39294E+01	7.62635E−02	1.66551E+00	5.23388E−04
2.01621E−01.....	4.53526E+07	6.76634E+03	3.42422E+01	5.14520E−02	1.66542E+00	6.15979E−04
2.27095E−01.....	4.36030E+07	5.11622E+03	2.63950E+01	4.17573E−02	1.66542E+00	8.55765E−04
2.52021E−01.....	4.19506E+07	4.01399E+03	2.02715E+01	3.52018E−02	1.66551E+00	1.06521E−03
2.90019E−01.....	3.95792E+07	3.31986E+03	1.33762E+01	2.67010E−02	1.66569E+00	1.24912E−03
3.27903E−01.....	3.74270E+07	2.79850E+03	8.76112E+00	1.94585E−02	1.66593E+00	1.30605E−03
3.65873E−01.....	3.54922E+07	2.38388E+03	5.72924E+00	1.34765E−02	1.66609E+00	1.32057E−03
4.03759E−01.....	3.37380E+07	2.05408E+03	3.77078E+00	9.05253E−03	1.66590E+00	1.30249E−03
4.41725E−01.....	3.21328E+07	1.92635E+03	2.50272E+00	5.97644E−03	1.66573E+00	1.26167E−03
4.79653E−01.....	3.06602E+07	1.65346E+03	1.68048E+00	3.92439E−03	1.66558E+00	1.20028E−03
5.17591E−01.....	2.92897E+07	1.47936E+03	1.14214E+00	2.59164E−03	1.66570E+00	1.12008E−03
5.55534E−01.....	2.79934E+07	1.48527E+03	7.85515E−01	1.72961E−03	1.66571E+00	1.02829E−03
5.93468E−01.....	2.67442E+07	1.41520E+03	5.46543E−01	1.17043E−03	1.66564E+00	9.32667E−04
6.31376E−01.....	2.55149E+07	1.30023E+03	3.84837E−01	8.05904E−04	1.66544E+00	8.38210E−04
6.69240E−01.....	2.42184E+07	1.27796E+03	2.74970E−01	5.65616E−04	1.66531E+00	7.46384E−04
7.06965E−01.....	2.26716E+07	1.40422E+03	2.00821E−01	4.06955E−04	1.66517E+00	6.53303E−04
7.19541E−01.....	2.20133E+07	1.54541E+03	1.82675E−01	3.68780E−04	1.66516E+00	6.22255E−04
7.32138E−01.....	2.13270E+07	1.59282E+03	1.66240E−01	3.34657E−04	1.66523E+00	5.90435E−04
7.44804E−01.....	2.06369E+07	1.51408E+03	1.50636E−01	3.03069E−04	1.66529E+00	5.59747E−04
7.57440E−01.....	1.99494E+07	1.60979E+03	1.35981E−01	2.73225E−04	1.66533E+00	5.29440E−04
7.70062E−01.....	1.92624E+07	1.54903E+03	1.22338E−01	2.45603E−04	1.66543E+00	4.99415E−04
7.82731E−01.....	1.85644E+07	1.55268E+03	1.09494E−01	2.20125E−04	1.66557E+00	4.71405E−04
7.95369E−01.....	1.78693E+07	1.60056E+03	9.75258E−02	1.96246E−04	1.66569E+00	4.45765E−04
8.08017E−01.....	1.71624E+07	1.54036E+03	8.63885E−02	1.74422E−04	1.66579E+00	4.20638E−04
8.45936E−01.....	1.49914E+07	1.65047E+03	5.74269E−02	1.17902E−04	1.66671E+00	3.61961E−04
8.83841E−01.....	1.26732E+07	1.74022E+03	3.46354E−02	7.36665E−05	1.66729E+00	3.37905E−04
9.21650E−01.....	1.00831E+07	2.00392E+03	1.74318E−02	4.03160E−05	1.66707E+00	3.66728E−04
9.34217E−01.....	9.11157E+06	2.12779E+03	1.28852E−02	3.14810E−05	1.66581E+00	3.84937E−04

In the subsequent discussions, the profile of the solar sound speed obtained with MDI data using STD as the reference model is referred to as the "standard sound-speed profile." Similarly, the solar density profile inferred from MDI data using STD is referred to as the "standard density profile," and the solar Γ_1 profile inferred from MDI data using STD is referred to as the "standard Γ_1 profile."

Figure 5 shows $(\Delta c/c)_{\rm resol}$ for models NODIF and ROT when STD is used as the proxy Sun. The resolution errors are small, generally less than 0.02%–0.03%. However, the resolution errors are relatively large in the solar core and at the base of the convection zone. The large error in the core results from the fact that there are very few p-modes that sample this region well. This causes the averaging kernel to be relatively wide at this innermost volume. The even larger resolution error at the base of the convection zone is caused by the sharp gradient in $\delta c^2/c^2$ for the different models.

The rms difference between the sound-speed profile inferred using the ROT model as the reference model and the STD sound profile as the proxy Sun is 0.015%; the rms difference is 0.038% when the NODIF model is used as the reference model. The rms difference for the density profile is 0.080% when ROT is the reference model and 0.31% when NODIF is the reference model.

The errors are larger when NODIF is compared with STD than when ROT is compared with the STD model, which simply reflects the fact that the difference in sound-speed profiles between the STD and NODIF models is larger than the difference in sound-speed profiles between STD and ROT. This observation leads to the rather obvious conclusion that one can expect to get more accurate solar sound speeds by using reference models that have sound speeds that are similar to the Sun.

The errors in the inferred density are also shown in Figure 5. The errors in density are about an order of magnitude larger than the errors in the sound speed.

The errors in the inferred Γ_1 due to resolution effects are expected to be small. This is because in the region where we have been able to do the inversions ($r < 0.94\ R_\odot$), Γ_1 differences between most models and the Sun are very smooth (see, e.g., Basu et al. 1999). The only model that could cause large errors is model OLD.

6. STANDARD SOUND SPEEDS, DENSITIES, AND Γ_1

Table 2 lists the solar sound speed, density, and Γ_1 profiles obtained with the STD model using MDI data. These data may be useful for other applications. Therefore, we have made available machine-readable files in the format of Table 2, but with a denser radius grid.[2]

[2] Machine-readable files in the format of Table 2, but with a denser radius grid, are available at: http://www.sns.ias.edu/~jnb.

7. COMPARISON WITH THE STANDARD SOLAR MODEL

How well does the standard solar model, STD, agree with the different measurements of the sound speed? Is the difference, shown in Figure 2, between the STD model and each of the measurements larger or smaller than the differences between the measurements themselves (shown in Fig. 4)?

The rms difference between the STD sound speeds and the solar speeds is 0.069% for the MDI data, 0.069% for the GONG data, and 0.064% for the BiSON + LOWL data set. These results are averaged over all regions of the Sun for which good data are available, from 0.05 to 0.95 $R_\odot$. In all cases the agreement is excellent, although the STD model can and should be improved, especially near the base of the convective zone (see, e.g., the discussion below of the pre–main-sequence model, PMS, and the model including rotation, ROT). In the solar core, where the neutrinos are produced, the rms agreement is even slightly better: 0.062% for the MDI data, 0.061% for the GONG data, and 0.044% for the BiSON + LOWL data set.

For all three data sets, the sound speeds at the base of the convection zone of the STD model differ by about 0.2% from the helioseismological values. This discrepancy has been seen earlier with similar standard models (e.g., Gough et al. 1996; Bahcall et al. 1997b) and can be attributed to the lack of mixing in the model below the base of the convective zone. In the models, diffusion without mixing causes a sudden, local rise in the helium abundance below the base of the convective zone. The increase in helium abundance increases the mean molecular weight, thereby decreasing the sound speed (since $c^2 \propto T/\mu$, where T is the local value of the temperature and μ is the local mean molecular weight).

The rms density difference between the model and the Sun is within 1% (see Fig. 3*a*). For Γ_1, the rms difference between the STD model and the Sun is less than 0.1% (Fig. 3*b*). The somewhat larger difference in the core has been attributed to errors in the equation of state (see Elliott & Kosovichev 1998).

8. COMPARISON WITH VARIANT AND DEFICIENT MODELS

How well do the variant models discussed in § 3.2 and § 3.3 agree with the helioseismological measurements?

Figures 6 and 7 show the results of the inversions made using MDI (Fig. 6) and GONG and BiSON + LOWL (Fig. 7) data. For most of the models, the vertical scale for the fractional velocity differences has a range of a few tenths of

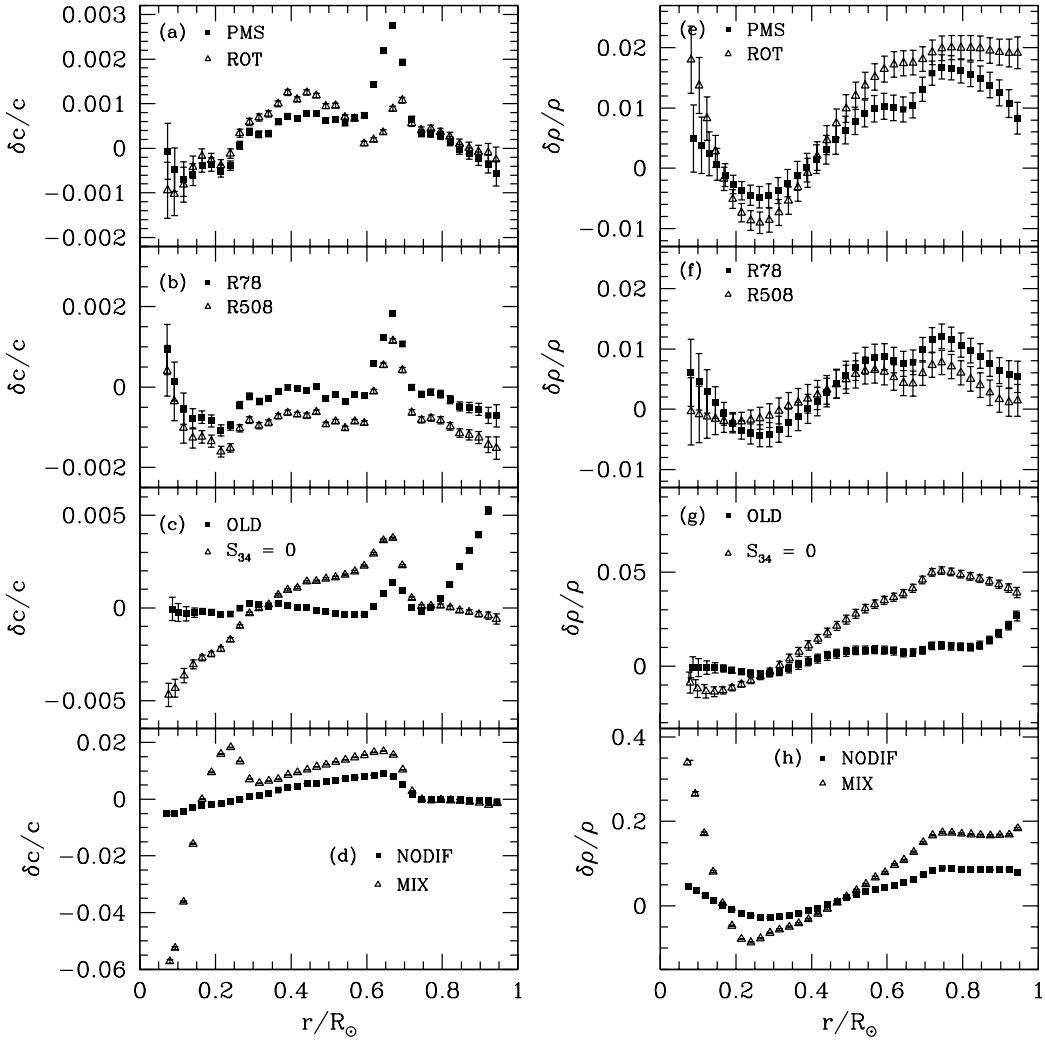

FIG. 6.—Relative sound-speed and density differences between the Sun and different solar models obtained using MDI data. The differences are in the sense (Sun − model)/model. Horizontal error bars are not shown for the sake of clarity. The differences are larger for the models described in panels *d* and *h*, and therefore the vertical scales cover a wider range for these panels. The different models are described in Table 1.

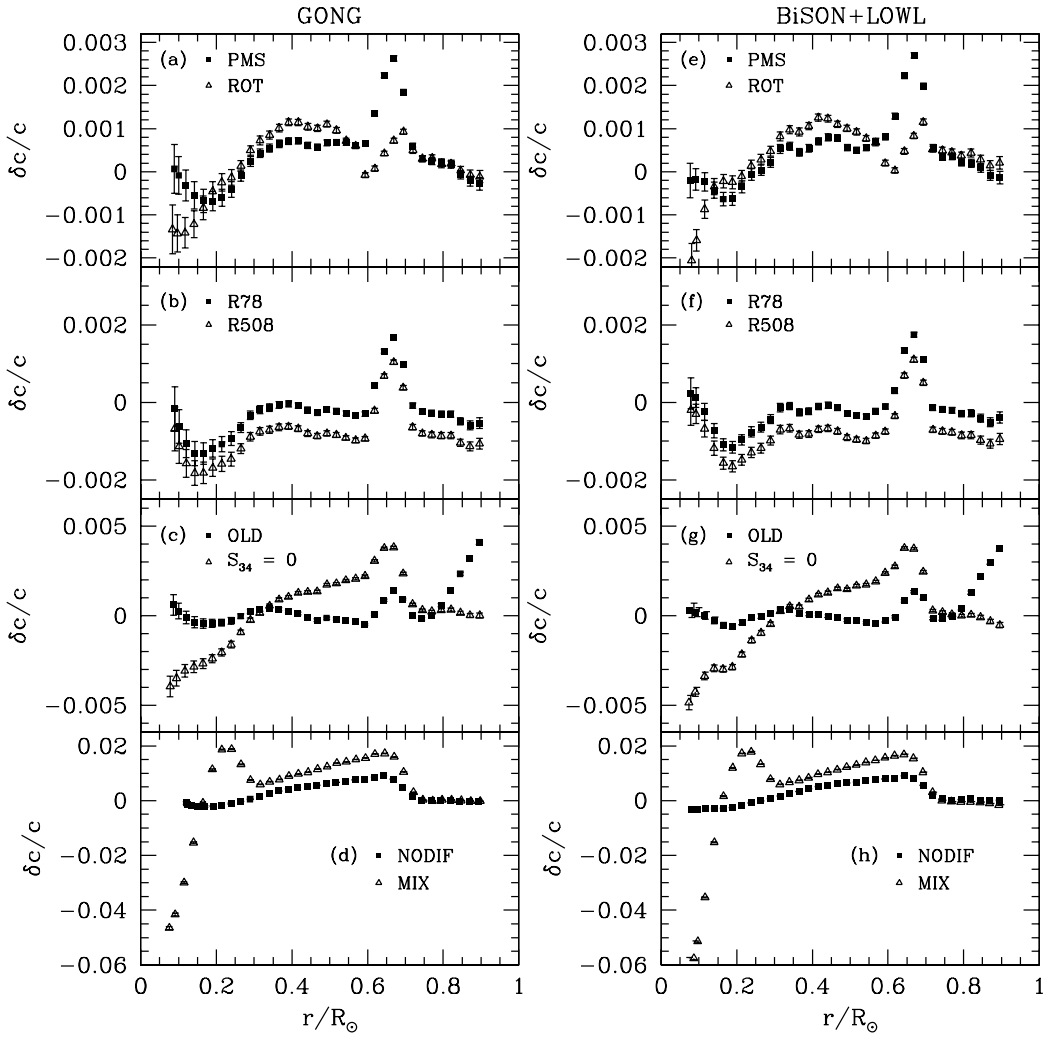

FIG. 7.—Relative sound-speed differences between the Sun and different solar models obtained using GONG and BiSON + LOWL data. The differences are larger for the models described in the panels *d* and *h*, and therefore the vertical scales cover a wider range for these panels. The different models are described in Table 1.

a percent. For the densities, the corresponding range is of the order of a few percent.

For Γ_1, Figure 8 shows the fractional differences between the Sun and the solar models found using MDI data. The fractional differences are less than or of the order of 0.2% for all the solar models except the MIX model. For the MIX model, the fractional differences are larger, of the order of 0.5%. We conclude that, with the exception of the MIX model, the theoretical profiles of Γ_1 are in good agreement with the solar values of Γ_1.

Table 3 summarizes the average rms deviation between the predicted sound-speed profile of the solar models discussed in § 3 and the measured sound-speed profile determined with the MDI data.

8.1. *Variant Models*

The pre–main-sequence model PMS yields values for $\delta c/c$ that are similar to the results obtained with the STD model (compare Figs. 6*a*, 7*a*, and 7*e* with Figs. 2*a*–2*c*). This similarity is to be expected, since the difference between the STD and PMS models is small, of the order of hundredths of a percent in $\delta c/c$ everywhere, and of the order of a few

TABLE 3

THE RMS SOUND SPEED, DENSITY, AND ADIABATIC INDEX DIFFERENCES WITH RESPECT TO THE SUN

Model	$(\delta c/c)$ (%)	$(\delta\rho/\rho)$ (%)	$(\delta\Gamma_1/\Gamma_1)$ (%)
STD.....	0.069	0.942	0.087
PMS	0.085	0.929	0.082
ROT	0.069	1.404	0.084
R78	0.064	0.673	0.090
R508	0.098	0.408	0.126
OLD	0.170	0.905	0.126
$S_{34} = 0$	0.209	3.108	0.146
NODIF.....	0.447	5.303	0.093
MIX	1.795	13.319	0.341

NOTE.—This table lists the percentage differences between the variables determined with the MDI data and those predicted by different solar models considered in the text (see § 3.2). The first four rows show values for variant standard models; the last four rows show different deficient (or nonstandard) models. This table shows how different each of the models is from the Sun.

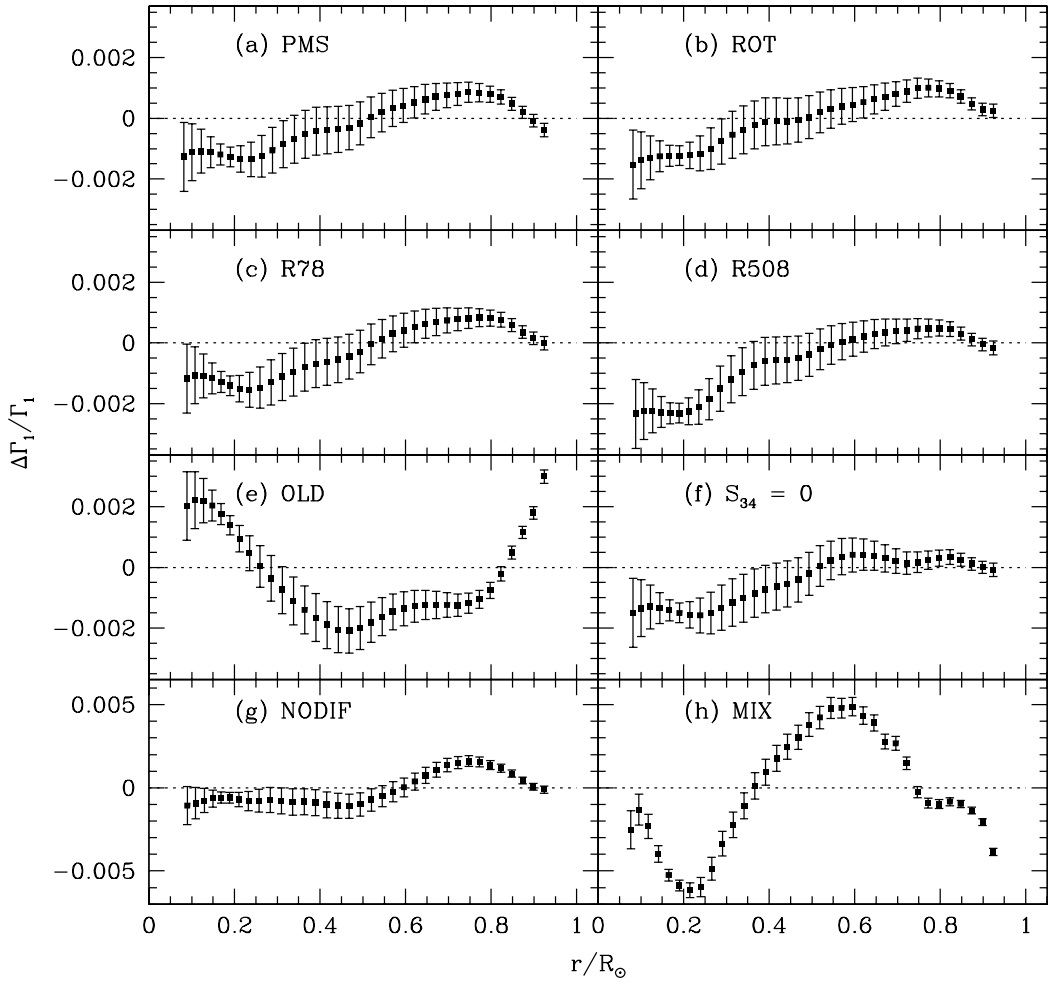

FIG. 8.—Relative Γ_1 differences between the Sun and different solar models obtained using MDI data. This figure is similar to Fig. 6, but showing Γ_1 instead of sound speed and density. The vertical scale of panels *g* and *h* is larger than the other panels in order to accommodate the large difference for model MIX (panel *h*).

tenths of a percent in $\delta\rho/\rho$ (see Figs. 1*a* and 1*d*). The difference in Γ_1 between the PMS model and the Sun is similar to that between the STD and the Sun (see Figs. 3*b* and 8*a*).

The model with rotational mixing, ROT, agrees better than the STD and PMS models with the helioseismological measurements near the base of the convective zone (see Figs. 6*a*, 6*e*, 7*a*, and 7*e*). This improved agreement confirms the suggestion (see Richard et al. 1996) that mixing at the base of the convection zone is a possible explanation for the significant discrepancy in this region between the measured and the STD model sound speeds. However, with this version of mixing, the agreement is slightly worse in the solar core, resulting in an overall rms deviation that is essentially the same as for the STD model. The difference in Γ_1 between ROT and the Sun is very similar to differences in Γ_1 found with models STD and PMS.

The two models with slightly different radii, R78 and R508, yield results (see Table 3) for the rms agreement with the MDI data that are comparable to the STD model. The R78 model yields slightly better agreement and the R508 model yields slightly worse agreement than is obtained with the standard model radius. The shape of the sound-speed differences between the R78 and R508 models and the Sun is very similar to the shape of sound-speed differences between the STD model and the Sun, but for the "nonstandard" radii the sound speeds are shifted downward in Figures 6*b*, 7*b*, and 7*f* (see also Figs. 9*c* and 9*d*).

8.2. *Comparison with Deficient Models*

The model constructed using old input data, OLD, produces a significantly worse rms sound speed discrepancy—0.17%, compared to 0.07% for the STD model (see Table 3). It is encouraging that the improvements in nuclear physics, equation of state, and radiative opacity described in § 3.1 have resulted in better agreement, by about a factor of 2, with the measured sound speeds. The OLD model also shows a larger difference relative to the Sun in Γ_1 toward the surface, confirming our suspicion that the equation of state used in the OLD model is not sufficiently accurate for optimal helioseismological applications.

The model with $S_{34} = 0$ does not allow the nuclear reaction $^3\mathrm{He}(\alpha, \gamma)^7\mathrm{Be}$. This change in the nuclear physics results in a sufficiently large modification in the structure of the solar core in the model that the difference is easily seen in precise helioseismological measurements (see Bahcall et al. 1997b). Figures 6*c*, 7*c*, and 7*g* show that the sound speed predicted by the $S_{34} = 0$ model differs from the helioseismologically inferred sound speeds by as much as 0.5% in the solar core, about an order of magnitude worse agreement than is obtained for the core with the STD model. The

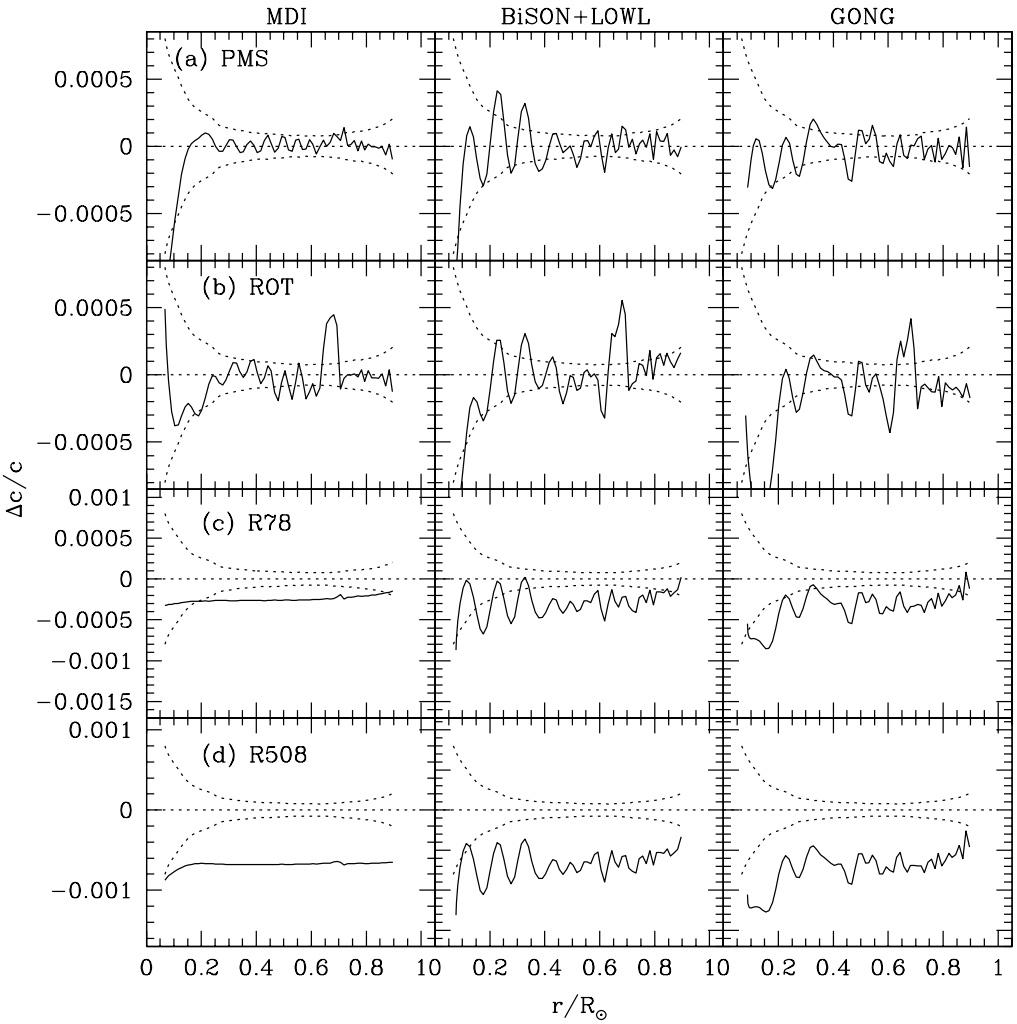

FIG. 9.—Fractional difference between the solar sound speed inferred using the STD solar model as a reference model and the sound speed obtained using each of four variant solar models as a reference model. For the reference sound profile, the MDI data set was inverted. Differences in the inferred sound speeds are presented for all three data sets, MDI, BiSON + LOWL, and GONG, and for all of the variant solar models. The 1 σ error envelope due to data measurement errors is shown by the dotted line.

influence of the reaction is seen even more dramatically in the density differences with respect to the Sun. Figure 6*g* shows that the discrepancies in density are as large as 5% in the outer region of the Sun. This result can be understood as follows. To achieve the same luminosity, the density in the core must increase when an important nuclear reaction, ^{3}He(α, γ)^{7}Be, is artificially set equal to zero. Since mass is conserved, any change in the density in the core must be compensated for by an opposite, larger change in the less dense outer layers. The small reduction relative to the STD model in the density at the core of the $S_{34} = 0$ solar model results in a relatively large change in the density of the outer layers and a significant discrepancy with the helioseismologically inferred density profile. Since the equation of state used in this model is the same as in STD, the differences in Γ_1 between this model and the Sun are very similar to those found with the STD model.

The model NODIF is generally a poor fit to the helioseismological measurements. Figures 6*d*, 6*h*, 7*d*, and 7*h* show that the disagreement is consistently large near the base of the convective zone, which reflects the fact that omitting diffusion results in models with incorrect depths of the convection zone (Bahcall & Pinsonneault 1995; see also Table 1 of the present paper). The rms discrepancy between the sound speeds of the NODIF model and the measured sound speeds is 6.5 times worse on averaged over the Sun than for the STD model. In the region where we have inverted for Γ_1 difference, NODIF fares quite well. The main difference in Γ_1 between the NODIF model and the Sun is expected to arise because of differences in helium abundance. However, that difference will show up only in the helium ionization zone (around 0.98 $R_\odot$), which we have not resolved.

The vertical scale for $\delta c/c$ must be increased by a factor of 25, from 0.002 to 0.05 (negative discrepancy) in order to display the very large discrepancy that exists for the MIX models. The differences are particularly glaring in the core, where the model is fully mixed. The sound-speed difference between the MIX model and the measurements is as much as 5% in the solar core, while the density difference is almost 40%. The corresponding maximal differences for the standard model in the solar core are 0.1% in $\delta c/c$ and 1% in $\delta\rho/\rho$, about 50 and 40 times smaller, respectively, than for the MIX model. The average rms discrepancy for the MIX model is about 25 times larger than for the STD model. Obviously, this model is not a good model of the Sun,

although it was proposed (Cumming & Haxton 1996) as a way of decreasing (but not eliminating) the differences between standard neutrino flux predictions and the measured neutrino fluxes. We were unable to obtain a reliable inversion for Γ_1 with model MIX because of the large difference in density between the model and the Sun.

9. DEPENDENCE ON THE ASSUMED REFERENCE MODEL

In this section, we evaluate the dependence of the inferred sound-speed profile and the inferred density profile on the assumed reference model. We calculate the sound speed or the density using two different combinations of reference model and measurement data, and then compare the results. Thus, we evaluate the set of differences formed by $(\text{model}_i - \text{data}_k) - (\text{model}_j - \text{data}_j)$, where for convenience we always take model_j as the STD model and data_j as the MDI data set, but model_i can be any one of the eight variant models discussed in § 3.2, and data_k is either the MDI, the BiSON + LOWL, or the GONG data set.

The principal results of this section are summarized in Table 4.

9.1. *Dependence of Sound Speed Profile on the Reference Model*

Figures 9 and 10 show the relative differences (double differences in the sense defined above) between the standard sound-speed profile (obtained with the model STD and MDI data) and the solar sound speed inferred using the eight variant models. We present result for all three of the data sets: MDI, BiSON + LOWL, and GONG.

The fractional difference, $\Delta c/c$, that is shown in Figures 9 and 10 is defined explicitly by the relation

$$\frac{\Delta c}{c} = \frac{c_{\odot,\,\text{variant}} - c_{\odot,\,\text{STD}}}{c_{\odot,\,\text{STD}}} \,. \tag{12}$$

The quantities $c_{\odot,\,\text{variant}}$ and $c_{\odot,\,\text{STD}}$ are the best estimates for the solar sound speed found using the specified reference model and data set. More explicitly, $c_{\odot,\text{model}} = c_{\text{model}}[(1 + \delta c^2/c^2)_{\text{model}}]^{1/2}$, where $(\delta c^2/c^2)_{\text{model}}$ is obtained directly from the inversion equation (6).

The inversions obtained using the PMS, ROT, OLD, and $S_{34} = 0$ models all yield sound speeds that differ from the standard sound-speed profile by only a few hundredths of a percent, i.e., within the errors due to the measurements (see Table 4 and Figs. 9 and 10). The only conspicuous exception occurs near the base of the convective zone, where the finite resolution causes a difference that is larger than the recognized measurement errors (see Fig. 9*b*).

The largest systematic, monotonic differences, $\sim 0.03\%$–0.08%, are found for models R78 and R508 (see Figs. 9*c* and 9*d*), although other models have larger rms differences (see Table 4). The sound-speed profiles obtained using these two models as reference models (and the MDI data for the measurements) exhibit a smooth difference with respect to the standard sound-speed profile. Data errors and resolution errors are not important when the MDI data are used for both the standard and the variant model inversions. One can see the irregular effects of using different data sets with finite resolution in the BiSON + LOWL and GONG panels of Figs. 9*c* and 9*d*. Equation (3) is obtained by assuming that there is no difference in radius between the Sun and the model; hence, a difference in the radius between the model and the Sun can introduce a systematic error in the inversion results. One must use an accurate value for the solar radius in order to obtain precisely correct inversion results (see Antia 1998; Basu 1998).

Even when the NODIF model is used as the reference model, the inferred sound-speed profile is in reasonable agreement with the standard profile except near the base of the convective zone. At the base of the convective zone, the combined effect of finite resolution and nonlinear effects increases the velocity difference well beyond what is expected from measurement errors alone. The results for the NODIF model are shown in Figure 10*c*.

The linear inversion fails for the MIX model in the solar core and near the base of the convective zone (see Fig. 10*d*). The rms fractional differences, $\Delta c/c$, are $\sim 0.4\%$ (see Table 4), an order of magnitude larger for the MIX model than for the models that more closely resemble the STD model. This failure is not surprising, since the MIX model is very different from the Sun (and the STD model) in the core and at the base of the convective zone. What is more remarkable is that despite the very large difference between the reference model and the Sun, the linear inversion scheme yields sound speeds for much of the solar volume that are within a few

TABLE 4

DEPENDENCE ON REFERENCE MODEL

	$\Delta c/c$			$\Delta\rho/\rho$	$\Delta\Gamma_1/\Gamma_1$
	MDI	BiSON + LOWL	GONG	MDI	MDI
MODEL	(%)	(%)	(%)	(%)	(%)
(1)	(2)	(3)	(4)	(5)	(6)
PMS	0.0246	0.0256	0.0131	0.2245	0.0124
ROT	0.0179	0.0321	0.0373	0.3067	0.0251
R78	0.0253	0.0345	0.0415	0.1361	0.0150
R508	0.0685	0.0700	0.0781	0.3077	0.0476
OLD	0.0190	0.0250	0.0125	0.2206	0.1401
$S_{34} = 0$	0.0224	0.0251	0.0226	1.5556	0.0231
NODIF.....	0.0734	0.0465	0.0826	1.8858	0.0543
MIX	0.4112	0.5078	0.3948	3.3593	0.2899

NOTE.—This table gives the rms differences in solar sound speed, density, and adiabatic index obtained using different reference models between radii of 0.07 and 0.9 $R_\odot$. See the introduction to § 9 for the definition of how the reference model dependence is calculated.

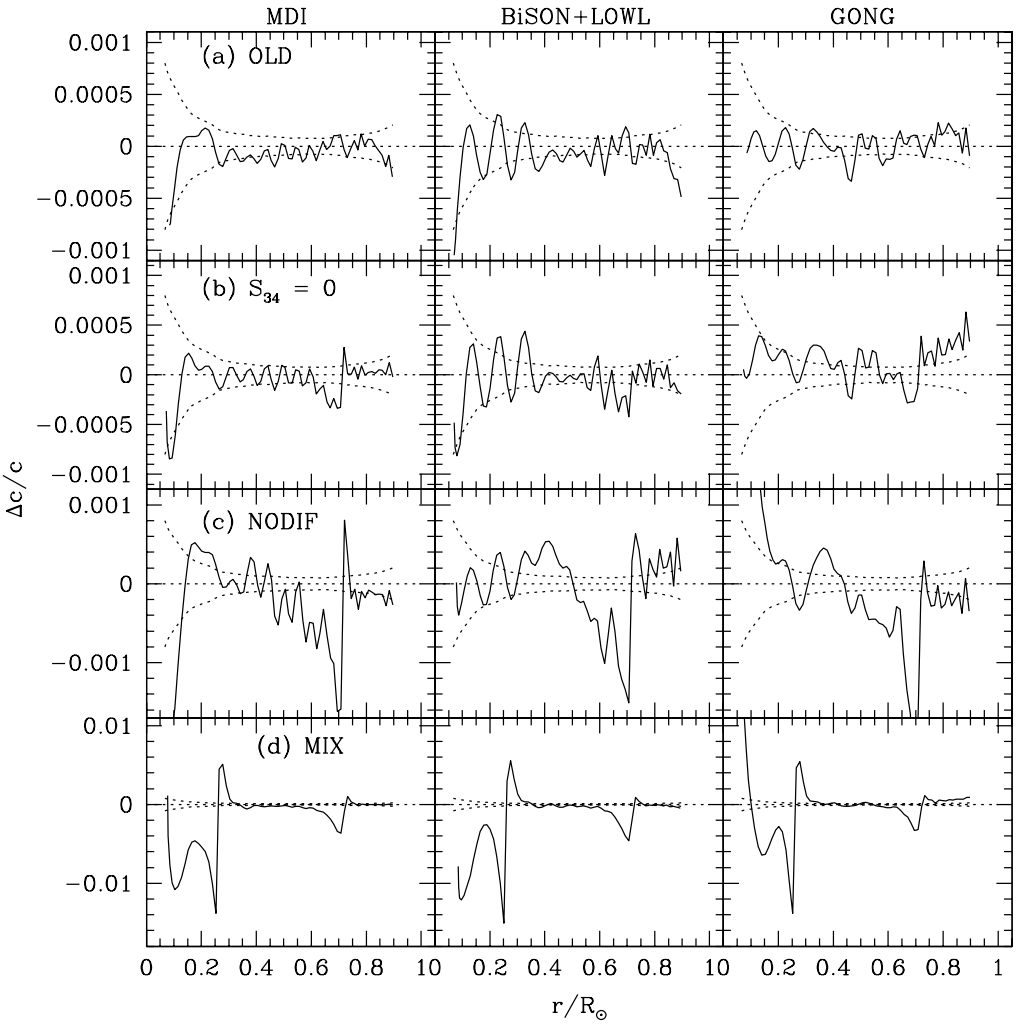

FIG. 10.—Same as Fig. 9, but for four solar models with considerably different physics than the STD model. The fractional differences obtained using the MIX model as the standard model are an order of magnitude larger than for the other cases considered; therefore, the vertical scale for the bottom panel covers an order of magnitude larger range.

tenths of a percent of the results obtained using much better reference models.

9.2. *Dependence of the Inferred Density Profile on the Reference Model*

Figure 11 shows the dependence of the inferred density profile on the assumed reference model. We are able to make these comparisons only for one data set, the MDI, since we were not able to make satisfactory inversions for the density profile using the other data sets.

For the PMS, ROT, R78, R508, and OLD models, which differ from each other by only modest amounts, the dependence of the inferred density profile on the assumed reference model is moderately large, of the order of 0.2% (see col. [5] of Table 4), but it is nevertheless generally smaller than the estimated measurement uncertainties. Of course, this dependence on the reference model is about an order of magnitude larger than the dependence of the sound speeds on reference models (see above).

For the NODIF, $S_{34} = 0$, and MIX models, the dependences shown in Figure 11 are much larger than the measurement errors, i.e., they are $\sim$a few percent. Nonlinear effects are clearly important in these inversions. Nevertheless, the most remarkable fact may be that despite the very significant differences between the variant models (NODIF, $S_{34} = 0$, and MIX) and the STD model, the different models all yield estimates for the solar density that agree with each other to within a few percent.

9.3. *Dependence of the Inferred Γ_1 Profile on the Reference Model*

Figure 12 shows the dependence of the inferred Γ_1 profile on the assumed reference model. All the comparisons are for the MDI data set.

For models PMS, ROT, R78, R508, and $S_{34} = 0$, the Γ_1 profiles obtained agree well with the Sun and with each other ($\sim$a few hundredths of a percent; see the last column of Table 4 for the rms dependence on the reference model). Although the structure of the $S_{34} = 0$ model is quite different from the Sun (and model STD), the structural difference is not large enough to cause major problems with the Γ_1 inversion. The Γ_1 profile obtained with model NODIF shows a moderately large difference, 0.05%. The profile obtained with model OLD shows an even larger difference, which we believe is due to an inadequate description of the structure close to the solar surface. By far the largest differ-

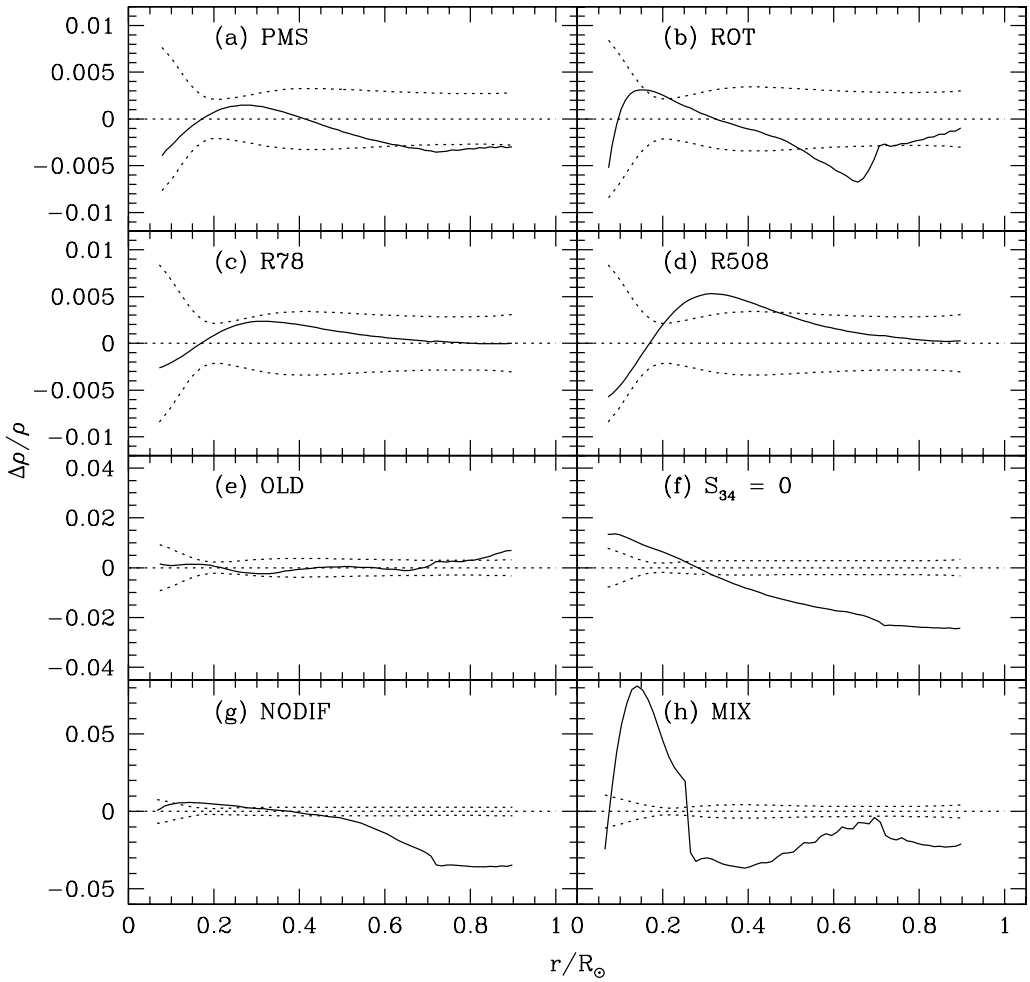

FIG. 11.—Relative errors in the solar density obtained using different reference models and the MDI data set. The reference solar density used to compute the differences is that obtained using model STD as the reference model. The 1 σ error envelope due to data errors is shown by the dotted line. The differences are larger for the models described in panels *e–h*, and therefore the vertical scales cover a wider range for these panels.

ences are found for model MIX, a result of the large difference in structure between this model and the Sun.

10. DISCUSSION

The principal purpose of this paper is to explore some of the systematic uncertainties that affect the determination of the profiles of the solar sound speed and the solar density.

As a by-product of this investigation, we have confirmed that standard solar models are in remarkable agreement with helioseismological measurements of the Sun. For example, the rms difference between the standard solar model profile for sound speeds and the helioseismological profile is only 0.07% (see discussion in § 7). Including pre–main-sequence evolution or a small amount of rotationally induced mixing does not affect the average results very much, but can give better agreement with observations near the base of the convection zone (see discussion in § 8).

Table 3 shows that five state-of-the-art solar models (STD, PMS, ROT, R78, and R508), each constructed with some different physics or parameter choice, all give comparable agreement with the global helioseismological measurements. On the basis of the global seismological evidence, we cannot say that one of these models is definitely more like the Sun than the others.

10.1. *Systematic Uncertainties*

10.1.1. *Uncertainties in the Data*

In § 4 we determine the systematic differences due to the choice of the individual data set by comparing sound-speed profiles calculated using different data sets. The results are shown in Figure 4; the difference between the results from state-of-the-art data sets is rms $\sim$ 0.02% averaged over the Sun, and bounces around within the 2 σ error envelopes determined by the combined measurement errors.

10.1.2. *Effects of Finite Resolution*

In § 5 we estimate the uncertainties due to the finite resolution of the inversion kernel by adopting a particular solar model as a proxy Sun and then comparing the convolved and inverted sound-speed (or density) profile with the true profile in the proxy Sun. The finite resolution of the inversion kernel leads to rms systematic uncertainties in the range $\sim$0.02%–0.04% in the profile of the sound speed, although the errors are typically much larger in the solar core and at the base of the convective zone (see Fig. 5). The uncertainties in the density profile due to finite resolution are typically an order of magnitude larger than the errors in the profile of the sound speed.

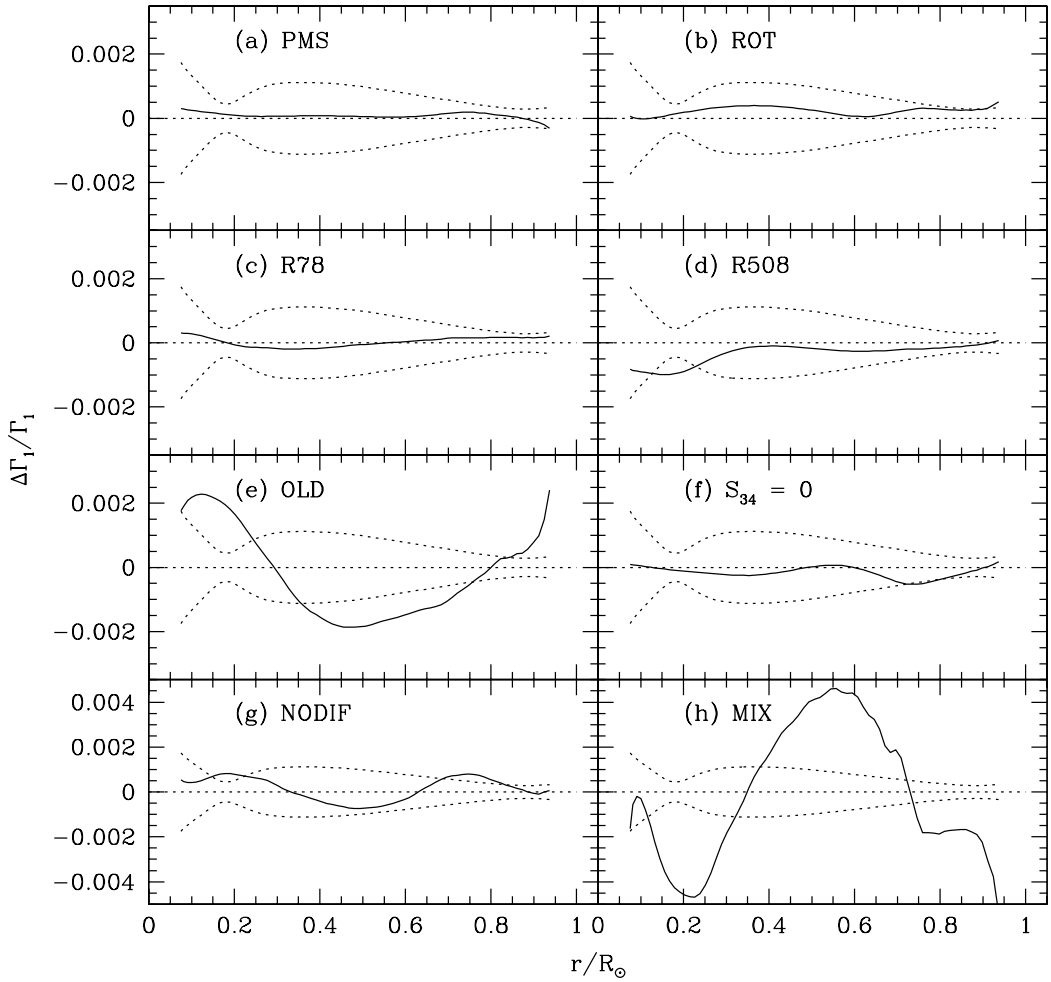

FIG. 12.—Relative errors in the adiabatic index Γ_1 for the Sun, obtained using different reference models and the MDI data set. The reference solar density used to compute the differences is that obtained using model STD as the reference model. The 1 σ error envelope due to data errors is shown by the dotted line. The differences are larger for the model described in panel *h*, and therefore the vertical scales cover a wider range for panels *g* and *h*.

10.1.3. *Uncertainties Due to Reference Models*

We use nine different solar models to determine the effects of the choice of reference model on the inferred sound speed, density, and Γ_1 profiles (see the discussion in § 9). The results are summarized in Table 4.

We have performed calculations for a standard solar model (STD) and four variant models (PMS, ROT, R78, and R508, each described in § 3.3). All five of these models include physics and input parameters that are state-of-the-art for 1999 solar models. The average rms difference between the sound velocities of each of the variant models and the STD model is 0.07% (see § 3.2). The average rms difference between the sound-speed profile inferred for the Sun using one of the variant models and the STD model is 0.03% (averaging the first four rows of Table 4). Hence, the spread among the inferred solar sound speeds is more than a factor of 2 less than the spread among the reference models themselves.

We also performed calculations for four deficient models (OLD, $S_{34} = 0$, NODIF, and MIX). The physics used in constructing each of these models is deficient in some significant way (see § 3.3). These deficiencies are reflected in the fact that the average rms difference between the sound velocities of each of the four nonstandard models and the STD model is 0.7% (cf. § 3.3), an order of magnitude larger than for the variant models. Nevertheless, when used as reference models, these deficient-by-design models give reasonably accurate values for the inferred solar sound speeds. The average rms difference between the sound-speed profile inferred for the Sun using one of the deficient models and the STD model is 0.13% (averaging the last four rows of Table 4). Thus, the discrepancy, when averaged over the different deficient models, is a factor of more than 5 less than the spread among the reference models.

Our bottom line on the systematic uncertainties for sound speeds is that, as expected, even relatively crude reference models yield reasonably good estimates for the solar sound speed.

Tables 3 and 4 show that the profile of Γ_1 is determined with a precision that is similar to, or slightly better than, the profile of the solar sound speed; that is, to an accuracy of $\sim 0.1\%$. The density is determined with an order of magnitude less precision, $\sim 1\%$.

10.2. *Can Helioseismology Rule Out Some Nonstandard Solar Models?*

What models are strongly disfavored (ruled out) by the helioseismological data? We choose as a figure of merit (crudely analogous perhaps to 1 standard deviation) the

largest rms difference in sound-speed profile between the Sun and one of the variant (state-of-the-art) solar models. This rms difference is 0.1% (for the R508 model; see Table 3). The $S_{34} = 0$ model has approximately twice as large a deviation (0.2%) and is therefore somewhat disfavored, but the OLD model (1995 physics) is perhaps still within the range of acceptability. Two models are strongly disfavored (ruled out at a high significance level). The no-diffusion model, NODIF, has a 0.45% rms difference in sound-speed profile with respect to the Sun; this is 4.5 times worse than the least successful of the variant models. The model with a mixed solar core, MIX (Cumming & Haxton 1996), has a rms difference of 1.8%, 18 times worse than the least successful of the variant models. We therefore conclude that the no-diffusion model and the mixed model are ruled out at a high level of significance.

J. N. B. is supported in part by NSF grant PHY 95-13835. M. P. is supported in part by NSF grant AST 97-31621 We are grateful to Pawan Kumar for valuable discussions and suggestions and to an anonymous referee for helpful comments on the initial manuscript. This work utilizes data from the Solar Oscillations Investigation/ Michelson Doppler Imager (SOI/MDI) on the *Solar and Heliospheric Observatory* (*SOHO*). *SOHO* is a project of international cooperation between ESA and NASA. This work also utilizes data obtained by the Global Oscillation Network Group (GONG) project, managed by the National Solar Observatory, a Division of the National Optical Astronomy Observatories, which is operated by AURA, Inc. under a cooperative agreement with the National Science Foundation. The data were acquired by instruments operated by the Big Bear Solar Observatory, High Altitude Observatory, Learmonth Solar Observatory, Udaipur Solar Observatory, Instituto de Astrofisico de Canarias, and Cerro Tololo Inter-American Observatory. We would like to thank the Birmingham Solar Oscillation Network (BiSON) and the LOWL instrument group for permission to use their data. BiSON is funded by the UK Particle Physics and Astronomy Research Council.

REFERENCES

Adelberger, E. C., et al. 1998, Rev. Mod. Phys., 70, 1265
Alexander, D. R., & Ferguson, J. W. 1994, ApJ, 437, 879
Antia, H. M. 1998, A&A, 330, 336
Antia, H. M., & Basu, S. 1994, A&AS, 107, 421
Antia H. M., & Chitre, S. M. 1998, A&A, 339, 239
Bahcall, J. N. 1989, Neutrino Astrophysics (Cambridge: Cambridge Univ. Press), chap. 11
Bahcall, J. N., Bahcall, N. A., & Shaviv, G. 1968, Phys. Rev. Lett., 20, 1209
Bahcall, J. N., Basu, S., & Kumar, P. 1997a, ApJ, 485, L91
Bahcall, J. N., Basu, S., & Pinsonneault, M. H. 1998, Phys. Lett. B., 433, 1
Bahcall, J. N., & Glasner, A. 1994, ApJ, 437, 485
Bahcall, J. N., & Pinsonneault, M. H. 1992, Rev. Mod. Phys., 64, 885
———. 1995, Rev. Mod. Phys., 67, 781
Bahcall, J. N., Pinsonneault, M. H., Basu, S., & Christensen-Dalsgaard, J. 1997b, Phys. Rev. Lett., 78, 171
Bahcall, J. N., & Ulrich, R. K. 1988, Rev. Mod. Phys., 60, 297
Balmforth, N. J. 1992, MNRAS, 255, 632
Basu, S. 1998, MNRAS, 298, 719
Basu, S., & Antia, H. M. 1997, MNRAS, 287, 189
Basu, S., Chaplin, W. J., Christensen-Dalsgaard, J., Elsworth, Y., Isaak, G. R., New, R., Schou, J., Thompson, M. J., & Tomczyk, S. 1997, MNRAS, 292, 243
Basu, S., Christensen-Dalsgaard, J., Pérez Hernández, F., & Thompson, M. J. 1996, MNRAS, 280, 651
Basu, S., Däppen, W., & Nayfonov, A. 1999, ApJ, 518, 985
Brown, T. M., & Christensen-Dalsgaard, J. 1998, ApJ, 500, L195
Chandrasekhar, S. 1964, ApJ, 139, 664
Chaplin, W. J., Elsworth, Y., Howe, R., Isaak, G. R., McLeod, C. P., Miller, B. A., van der Raay, H. B., Wheeler, S. J., & New, R. 1996, Sol. Phys., 168, 1
Choi, P. I., & Herbst, W. 1996, AJ, 111, 283
Cox A. N., & Kidman R. B. 1984, in Theoretical Problems in Stellar Stability and Oscillations, ed. P. Ledoux (Liége: Inst. d'Astrophysique), 259
Cumming, A., & Haxton, W. C. 1996, Phys. Rev. Lett., 77, 4286
Däppen, W., Gough, D. O., Kosovichev, A. G., & Thompson, M. J. 1991, in Challenges to Theories of the Structure of Moderate-Mass Stars, ed. D. O. Gough & J. Toomre (Berlin: Springer), 111
Dziembowski, W. A., Pamyatnykh, A. A., & Sienkiewicz, R. 1990, MNRAS, 244, 542
Elliott, J. R. 1996, MNRAS, 280, 1244
Elliott, J. R., & Kosovichev, A. G. 1998, ApJ, 500, L199
Gough, D. O. 1993, in Astrophysical Fluid Dynamics: Les Houches Session XLVII, ed. J.-P. Zahn & J. Zinn-Justin (Amsterdam: Elsevier), 399
Gough, D. O., et al. 1996, Science, 272, 1296
Grevesse, N., & Noels, A. 1993, in Origin and Evolution of the Elements, ed. N. Prantzos, E. Vangioni-Flam, & M. Cassé (Cambridge: Cambridge Univ. Press), 15
Gruzinov, A., & Bahcall, J. N. 1998, ApJ, 504, 996
Guenther, D. B., Demarque, P., Kim, Y.-C., & Pinsonneault, M. H. 1992, ApJ, 387, 372
Iglesias, C. A., & Rogers, F. J. 1996, ApJ, 464, 943
Iglesias, C. A., Rogers, F. J., & Wilson, B. G. 1992, ApJ, 397, 717
Kippenhahn, R., & Thomas, H.-C. 1970, in Stellar Rotation, ed. A. Slettebak (Dordrecht: Reidel), 20
Korzennik, S. G., & Ulrich, R. K. 1989, ApJ, 339, 1144
Kosovichev, A. G. 1995, in ASP Conf. Ser. 76, Helio- and Asteroseismology from the Earth and Space, ed. R. K. Ulrich, E. J. Rhodes, & W. Däppen (San Francisco: ASP), 89
Kosovichev, A. G., et al. 1997, Sol. Phys., 170, 43
Krishnamurthi, A., Pinsonneault, M. H., Barnes, S., & Sofia, S. 1997, ApJ, 480, 303
Kurucz, R. L. 1991, in Stellar Astmospheres: Beyond Classical Models, ed. L. Crivellari, I. Hubeny, & D. G. Hummer (NATO ASI Ser. C, 341; Dordrecht: Kluwer), 441
Pijpers, F. P., & Thompson, M. J. 1992, A&A, 262, L33
Pinsonneault, M. H. 1997, ARA&A, 35, 557
Pinsonneault, M. H., Walker, T. P., Steigman, G., & Narayanan, V. K. 1999, ApJ, 527, 180
Proffitt, C. R. 1994, ApJ, 425, 849
Rabello-Soares, M. C., Basu, S., & Christensen-Dalsgaard, J. 1999, MNRAS, submitted
Rhodes, E. J., Jr., Kosovichev, A. G., Schou, J., Scherrer, P. H., & Reiter, J. 1997, Sol. Phys., 175, 287
Richard, O., Vauclair, S., Charbonnel, C., & Dziembowski, W. A. 1996, A&A, 312, 1000
Rogers, F. J., Swenson, F. J., & Iglesias, C. A. 1996, ApJ, 456, 902
Salpeter, E. E. 1954, Australian J. Phys., 7, 373
Schou, J., Kosovichev, A. G., Goode, P. R., & Dziembowski, W. A. 1997, ApJ, 489, L197
Takata, M., & Shibahashi, H. 1998, in Structure and Dynamics of the Sun and Sun-like Stars, ed. S. G. Korzennik & A. Wilson (ESA SP-418; Noordwijk: ESA), 543
Thoule, A. A., Bahcall, J. N., & Loeb, A. 1994, ApJ, 421, 828
Tomczyk, S., Schou, J., & Thompson, M. J. 1995a, ApJ, 448, L57
Tomczyk, S., Streander, K., Card, G., Elmore, D., Hull, H., & Caccani, A. 1995b, Sol. Phys., 159, 1
Tripathy, S. C., Basu, S., & Christensen-Dalsgaard, J. 1997, In IAU Symp. 181, Sounding Solar and Stellar Interiors, ed. J. Provost & F.-X. Schmider (Nice: Univ. Nice, Obs. de la Côte d'Azur), 129
Ulrich, R. K. 1982, ApJ, 258, 404

Note added in proof.—After the proofs of this paper were returned, we learned of work on the same topic by S. degl'Innocenti, W. A. Dziembowski, G. Fiorentini, & B. Ricci (Astropart. Phys., 7, 77 [1997]).